



HAL
open science

Monolith weak affinity chromatography for μ g-protein-ligand interaction study

Lucile Lecas, Jérôme Randon, Alain Berthod, Vincent Dugas, Claire
Demesmay

► **To cite this version:**

Lucile Lecas, Jérôme Randon, Alain Berthod, Vincent Dugas, Claire Demesmay. Monolith weak affinity chromatography for μ g-protein-ligand interaction study. *Journal of Pharmaceutical and Biomedical Analysis*, 2019, 166, pp.164-173. 10.1016/j.jpba.2019.01.012 . hal-02015987

HAL Id: hal-02015987

<https://hal.science/hal-02015987v1>

Submitted on 21 Oct 2021

HAL is a multi-disciplinary open access archive for the deposit and dissemination of scientific research documents, whether they are published or not. The documents may come from teaching and research institutions in France or abroad, or from public or private research centers.

L'archive ouverte pluridisciplinaire **HAL**, est destinée au dépôt et à la diffusion de documents scientifiques de niveau recherche, publiés ou non, émanant des établissements d'enseignement et de recherche français ou étrangers, des laboratoires publics ou privés.



Distributed under a Creative Commons Attribution - NonCommercial 4.0 International License

21 **Abstract**

22

23 Affinity monolith columns of 375 nL (effective length 8.5 cm, internal diameter 75 μ m) were
24 developed for protein-ligand affinity investigations needing only 3 μ g of human serum albumin
25 (HSA). To promote specific interactions and avoid non-specific ones, different combinations of
26 monolithic supports and bio-functionalization pathways were evaluated. Silica and
27 glycidylmethacrylate based monoliths were *in-situ* synthesized and grafted with HSA. Two direct
28 grafting methods epoxy-amine and Schiff Base plus the streptavidin-biotin method were compared.
29 The columns were evaluated by frontal analysis with ligands of known affinity for HSA. It is shown
30 that a classical capillary electrophoresis instrument equipped with an external pressure device can be
31 used to do weak affinity chromatography at low pressure (less than 1.2 MPa) in a fully automated
32 way and with very low reagent consumption. The grafting pathways were compared in terms of (i)
33 total and active amounts of immobilized protein, (ii) non-specific interactions, (iii) protein
34 denaturation. According to these criteria, the organic monoliths combined with the streptavidin-
35 biotin approach provided the best results. This immobilization pathway led to the highest active
36 protein content (40 pmol of HSA per 8.5-cm column) with less than 10% non-specific interactions and
37 84% protein activity. The target grafting step lasts only 10 min and is UV-monitored, the UV
38 breakthrough curve giving the exact amount of bound protein. This novel approach was validated by
39 K_d measurements of 3 known ligands of HSA. Streptavidin generic monolith columns could be stored
40 at 4°C for 3 months maintaining activity. μ g of a biotin modified sensitive protein could be attached
41 to a stable streptavidin monolith for immediate interaction studies avoiding stability problems. This
42 development was subsequently extended to another protein of higher pharmaceutical interest: the
43 N-terminal domain of HSP90. Affinity was measured for two known ligands and determined K_d values
44 were in accordance with the literature, proving that our technique is applicable to other proteins.

45

46 **Keywords:** weak affinity chromatography, miniaturization, monoliths, protein-ligand interaction,
47 HSA, HSP90

48

1. Introduction

49

50 Understanding and quantifying biomolecular interactions is at the very heart of life sciences. From a
51 fundamental point of view, it allows for a better understanding of biological processes. Biomedical
52 interactions are also needed for health applications, such as drug discovery applied to the
53 development of new therapeutic molecules [1]. Recently, weak affinity chromatography (WAC) has
54 been introduced as a chromatographic technique where biomolecules such as proteins are
55 immobilized on the stationary phase [2,3]. WAC has been increasingly used to study interactions in
56 biological systems [2–5]. The chromatographic retention of a ligand injected in WAC is linked to the
57 protein-ligand interaction strength. Hence, WAC can be used to obtain fundamental and/or
58 mechanistic information in a variety of fields such as: (i) chiral separations [6,7], (ii) fragment
59 screening in fragment-based drug discovery [3], (iii) selection of site-selective probe for use in the
60 high-throughput screening of drug binding to protein [8] and (iv) thorough thermodynamic and
61 kinetic studies of protein-ligand interaction [9,10]. A study reported that the data obtained by WAC
62 were coherent with what the more sophisticated NMR and Thermal Shift Assay techniques were
63 producing [5]. Since running cost is an important factor, WAC appears to be very competitive for
64 biomolecular interaction studies [3].

65

66 The WAC studies were mainly performed using “classical” columns with an internal diameters of 4.6
67 mm or 2.1 mm, a length varying from one to 20 cm, and using 5 μm silica particles with wide 30 nm
68 pore size [4,8,9,11–14]. Few studies were also conducted with silica monoliths at classical scale
69 (columns with a 4.6 mm i.d and with lengths ranging from a few centimeters [6] to a few millimeters
70 [15]), or with organic polymer monoliths (4.6 mm i.d., length from a few centimeters [16] to a few
71 millimeters [7]). The immobilization of the target protein onto the stationary phase allows for a
72 significant decrease of the amount of protein needed for the interaction studies compared to what
73 was needed with the *in vitro* solution studies. However, the preparation of a “classical” affinity
74 column can require up to a few dozen milligrams of the target protein. This amount is still significant.
75 Obtaining milligram amounts of stable and functionally folded proteins can be highly challenging. A
76 first attempt to reduce the amount of protein needed in the sub-milligram range was described by
77 the group of Ohlson who prepared 500 μm i.d. silica particles affinity columns [17]. Further down-
78 sizing the column diameter should allow using even less target protein (μg for 75 μm i.d.) but cannot
79 be straightforwardly achieved. The packing of 75 μm i.d. capillary columns is very difficult so
80 monolithic columns appear to be a viable alternative. Monoliths can be synthesized *in-situ* leading to

81 chromatographic capillary columns with high permeability. After the bare monolith synthesis, the
82 protein grafting step has to be in-situ performed by flowing the protein solution.

83 The numerous bio-functionalization pathways of chromatographic supports with a target protein
84 have been recently reviewed [18]. The simplest pathway is the direct covalent coupling of the
85 protein onto an epoxy ring via the reaction of the primary amine of a lysine side chain of the protein.
86 This grafting way has drawbacks: it is time-consuming (48 to 72 h) due to the low reactivity of the
87 epoxy moieties [7,16]. Among the reviewed grafting methods, the Schiff base method stands out
88 [7,16,19] as this method should produce 1.5 to 4 time higher grafting densities than the epoxy
89 method for similar reaction times [7,16]. Although the epoxy and Schiff base grafting methods have
90 proved to work well for model proteins such as HSA and few soluble proteins [3], they are less usable
91 with fragile proteins (that may partially denature during the time consuming grafting step) or with
92 proteins available in scarce amount (a great excess of protein is consumed). Therefore, we intended
93 to develop an alternative method overcoming such drawbacks and to compare it with the previously
94 reported methods. It relies on the instantaneous capture of the biotinylated-target protein onto a
95 streptavidin-modified support. The streptavidin-biotin interaction ($K_d=10^{-15}$ M [20]) should be strong
96 enough to support dynamic affinity studies under mild conditions.

97 In this study, silica-based and organic-based monolithic nano-columns were prepared, investigated
98 and compared in frontal analysis mode for nano-WAC applications. Human Serum Albumin (HSA) was
99 used as model target protein and grafted according to three different immobilization pathways,
100 namely: the epoxy-amine, Schiff base and streptavidin-biotin methods. The immobilization pathways
101 were considered in term of (i) amount of total and active protein per column, (ii) secondary non-
102 specific interactions and (iii) protein activity conservation. K_d were measured and compared to the
103 literature in order to validate this new approach. For the streptavidin-biotin grafting path the stability
104 of the columns was investigated in screening and storage conditions. After the development with
105 HSA as target model, nano-columns were grafted with the N-terminal domain of HSP90, in order to
106 confirm the applicability of our technique to another protein, and the K_d of three fragments (ligands)
107 were measured.

108

109 **2. Material and methods**

110 **2.1. Reagents and chemicals**

111 Ethylene dimethacrylate (EDMA, 97%), glycidyl methacrylate (GMA, 98%), 1-propanol, 1,4-
112 butanediol, (3-methacryloxypropyl)-trimethoxysilane (γ -MAPS), tetramethoxysilane (TMOS),
113 methytrimethoxysilane (MTMS), urea, polyethylene glycol (PEG, MW=10,000), methanol (HPLC

114 grade), triethylamine (TEA), sodium periodate, lithium hydroxide, dipotassium hydrogen phosphate
115 (K_2HPO_4), o-phosphoric acid, dimethylsulfoxide (DMSO), acetic acid, coomassie brilliant blue G (CBB),
116 (3-glycidyloxypropyl)trimethoxysilane (GPTMS), sodium cyanoborohydride, ibuprofen (racemic),
117 warfarin (racemic), furosemide, adenosine 5'-diphosphate sodium salt, n,n-diethylvanillamide, 3-
118 hydroxy-4-methoxybenzyl alcohol, magnesium chloride ($MgCl_2$), human serum albumin (HSA, fatty
119 acid free, globulin free, $\geq 99\%$), streptavidin (from *streptomyces avidinii*, affinity purified, $\geq 13 U \cdot mg^{-1}$
120 of protein), were purchased from Sigma Aldrich (L'Isle d'Abeau Chesne, France). Ammonia solution
121 (28-30 %) was from Merck (Darmstadt, Germany). Sulfuric acid (18 M) was from VWR (Fontenay-
122 sous-bois, France). All aqueous solutions were prepared using $>18 M\Omega$ deionized water. Preparation
123 of the phosphate buffer was done by dissolving 1.17 g of K_2HPO_4 in 100 mL of ultrapure water and pH
124 was adjusted to 7.4 with ortho-phosphoric acid. An EZ-LinkNHS-PEG4-Biotinylation Kit was purchased
125 from Thermo Scientific (VWR). HSP90 protein was produced by a partner laboratory (Institut de
126 Biologie et Chimie des Protéines, Lyon France). The N-terminal fragment of HSP90 (9-236) was
127 expressed in E.coli (BL21) with a histidine tag and purified by a monoQ column. Protein samples were
128 delivered at $6.7 mg \cdot mL^{-1}$ in PBS buffer and stored at $-80^\circ C$ before use.

129

130 **2.2. Instrumentation**

131 Liquid flow into capillary columns was driven by pressure gradient using the microfluidic flow
132 controller MFCS-EZ100 system (Fluigent, Villejuif, France). Inlet pressure values are reported to
133 specify the liquid flow conditions (outlet pressure was always set up at atmospheric pressure). An LC
134 pump L-6000 (Merck, Darmstadt, Germany) was used to rinse the freshly prepared capillaries in
135 pressure mode (3 MPa). Nano-LC experiments (frontal weak affinity chromatography experiments)
136 were carried out with a capillary electrophoresis Agilent HP3D CE system (Agilent Technologies,
137 Waldbronn, Germany) equipped with external pressure nitrogen supply allowing to work up to 1.2
138 MPa. System control and data acquisition were carried out using the Chemstation software (Agilent).

139

140 **2.3. Capillary monolith syntheses**

141 **2.3.1 Epoxy-functionalized silica monoliths**

142 Polyimide-coated fused-silica capillaries (75 μm i.d.) were purchased from Polymicro Technologies
143 (Molex, Phoenix, Arizona, USA). The silica monolith preparation was extensively described [21].
144 Briefly, a 18 mL mixture of TMOS/MTMS (85/15, v/v) was added to 40 mL 0.01 M acetic acid solution
145 containing 1.9 g PEG and 4.05 g urea. The sol mixture was stirred at $0^\circ C$ for 30 min. Then, the
146 temperature was raised to $40^\circ C$ and the mixture was loaded into 15-cm 75- μm i.d. fused-silica

147 capillary pieces. Next, the partially filled capillaries (approximately 10 cm on the total length of 15
148 cm), were end-plugged and kept at 40°C overnight for gelification. Mesopores were formed by urea
149 decomposition through gently raising the capillary temperature up to 120°C maintained for 4 h. After
150 cooling, the monoliths were thoroughly washed with methanol. GPTMS surface functionalization was
151 done by flushing monoliths with a solution containing 5 % of GPTMS and 2.5 % of TEA in
152 methanol/water (95/5, v/v). The reaction was conducted for 3 h at room temperature. Monoliths
153 were then rinsed with methanol for 30 min (0.7 MPa).

154 **2.3.2 Glycidyl methacrylate monoliths**

155 Fused-silica capillaries with UV transparent coating (TSH, 75- μm i.d.) were purchased from Polymicro
156 Technologies (Molex). A pre-treatment procedure was carried out in order to ensure a strong
157 covalent attachment of monoliths to capillary walls. Capillaries were flushed with a 5 % (v/v) solution
158 of γ -MAPS in methanol/water (95/5, v/v) with 2.5 % TEA for 1 h at 0.7 MPa. Next, they were rinsed
159 with methanol for 15 min at 0.7 MPa and dried at room temperature under nitrogen stream. A
160 polymerization mixture adapted from [22] was prepared by mixing 0.9 mL GMA, 0.3 mL EDMA, 1.05
161 mL 1-propanol, 0.6 mL 1,4-butanediol and 0.15 mL ultra-pure water. Prior to UV irradiation, potential
162 oxygen in the solution was removed by 15 min ultrasonication, and 12 mg of the initiator 2,2-
163 azobisisobutyronitrile were added under magnetic stirring. The pre-treated capillary was then filled
164 with the polymerization mixture under 0.1 MPa N_2 pressure. The photopolymerization reaction was
165 performed in a Bio-link UV cross-linker (VWR International, France) under 365 nm UV light for a total
166 energy of 6 $\text{J}\cdot\text{cm}^{-2}$. In order to localize the monolith inside the silica capillary, a PEEK tubing (380 μm
167 i.d.) was used as a mask to cover non-irradiated areas. After polymerization, the 8.5-cm monolithic
168 column segment of the 15-cm capillary was rinsed with methanol for 1 h using a LC pump in pressure
169 mode (3 MPa) to remove any unreacted reagents.

170

171 **2.4. Protein immobilization protocols**

172 **2.4.1 Direct coupling methods**

173 *2.4.1.1 Epoxy method*

174 Proteins can be directly immobilized onto epoxy-functionalized monolithic columns via reactions
175 involving primary amines ($-\text{NH}_2$), such as the lysine side-chains, or the amino-termini of proteins. This
176 grafting was carried out by circulating a 2 $\text{mg}\cdot\text{mL}^{-1}$ HSA solution in phosphate buffer (67 mM, pH 7.4)
177 for 48 h at 0.7 MPa. The column was then rinsed with phosphate buffer solution and stored at 4°C
178 prior to use.

179 *2.4.1.2 Schiff base method*

180 The Schiff base method consists in the reaction of aldehyde reactive surface groups of the solid
181 support with the amino-groups of the protein. Aldehyde reactive moieties are classically obtained by
182 oxidation of diol functions. First, the epoxy groups of the epoxy-functionalized silica or GMA-co-
183 EDMA monoliths were hydrolyzed into diols flowing 1 M sulfuric acid for 2 h at 0.7 MPa. After rinsing
184 all residual acid, the diol-monolith was oxidized to aldehyde using a 0.12 M NaIO_4 solution at pH 5.5.
185 Then a 2 mg.mL^{-1} HSA and 8 mg.mL^{-1} NaBH_3CN solution in 67 mM pH 6 phosphate buffer was
186 percolated through the column for 48 h at 0.7 MPa and room temperature. Sodium
187 cyanoborohydride reduces imine groups, a necessary treatment in order to get reliable
188 immobilization. After immobilization, the column was flushed with sodium borohydride (2.5 mg.mL^{-1} ,
189 phosphate buffer 67 mM pH 8 (2 h, 0.7 MPa) to reduce residual aldehydes. The HSA affinity columns
190 were then rinsed with phosphate buffer and stored at 4°C. The same protocol was used to evaluate
191 the impact of protein concentration (1 mg.mL^{-1} and 0.5 mg.mL^{-1} HSA were also tested) and grafting
192 duration (12 h instead of 48 h was tested) on final protein content.

193

194 **2.4.2 Streptavidin-biotin method**

195 The streptavidin-biotin method relies on the instantaneous capture of the biotinylated-target protein
196 onto a streptavidin-modified monolith. The affinity of the streptavidin-biotin interaction is so high (in
197 the femtomolar range, $K_d=10^{-15}$ M [20]) that this coupling may be considered as covalent.
198 Streptavidin was grafted on the organic monolith following the Schiff base method described above
199 using a 1 mg.mL^{-1} streptavidin solution. Coupling of biotin to HSA was done following the instructions
200 of the Thermo EZ-Link NHS-PEG4-Biotinylation Kit. Being a small molecule, biotin (M.W. 244 g.mol^{-1})
201 can be attached to many proteins without altering their biological activities [23]. The molar ratio of
202 NHS-PEG₄-biotin to protein was adjusted to obtain the desired level of incorporation. Biotin
203 incorporation (1.7 biotin/protein molecule) was estimated using the HABA assay. All excess of biotin
204 reagent was removed using a desalting column. The concentration of the resulting biotin-HSA
205 solution was calculated with the solution's absorbance at 280 nm ($\epsilon_{\text{HSA}}= 0.5982 \text{ L.g}^{-1}.\text{cm}^{-1}$). Finally, the
206 biotin-HSA solution was loaded through the streptavidin immobilized column using the Agilent CE
207 system at 1.2 MPa pressure, monitoring UV absorbance at 230 and 280 nm. The percolation was
208 stopped when saturation of the support was reached, i.e. the biotin-HSA reached the detector
209 (observation of a plateau at 230 and 280 nm). The breakthrough curve was used to estimate the
210 quantity of captured protein on the streptavidin immobilized support. Similar protocol was used for
211 the HSP90 protein. Biotin incorporation was 2.8 biotin/HSP90 N-ter and resulting biotinylated protein
212 concentration was calculated using $\epsilon_{\text{HSP90}}= 0.5822 \text{ L.g}^{-1}.\text{cm}^{-1}$.

213

214 2.5. Columns evaluation

215 Affinity columns were evaluated by frontal chromatography using a capillary electrophoresis system
216 (S.1). The experiments were conducted using the CE system in the so-called “short-end” injection
217 mode. The system was exclusively operated in the pressurization mode by applying external pressure
218 (no voltage applied). The inlet of the capillary column is simply immersed in the solution to be
219 infused and the external pressure forces the liquid to flow inside the capillary column. The detection
220 was achieved “on-column” (in an empty section of the 10-cm capillary located just after the
221 monolith), with a diode array detector operated in a multi-wavelength mode. The effective length
222 was 8.5 cm. Experiments were conducted under controlled room temperature (25°C). After every
223 analysis, the capillary column was rinsed with 20 column volumes of phosphate buffer to eliminate
224 the infused compounds.

225

226 **2.5.1 Determination of the number of actives sites (B_{act}) and protein-ligand dissociation** 227 **constant (K_d) by in-capillary frontal analysis**

228 The total number of actives sites (B_{act}) and the protein-ligand dissociation constant (K_d) were
229 evaluated by frontal analysis [8]. Different ligands of known affinity for HSA (Fig. 1) were selected to
230 characterize the columns : warfarin, furosemide and ibuprofen [6,11,24].

231 Fig.1.

232

233 10 mM stock solutions of the probe ligands were prepared in DMSO to ensure complete
234 solubilization. Solutions of increasing ligand concentration (5, 7, 10 and 20 μM) were prepared in
235 phosphate buffer (67 mM K_2HPO_4 , pH 7.4) and percolated at 1.2 MPa (about 240 $\text{nL}\cdot\text{min}^{-1}$ or 0.1 $\text{cm}\cdot\text{s}^{-1}$
236 for 8.5-cm length columns). The flow rate, F , was calculated using a non-retained solute or the
237 plateau of residual DMSO. Compounds were monitored at their characteristic wavelength (DMSO
238 214 nm, warfarin 308 nm, furosemide 280 nm, and ibuprofen 230 nm). The accurate determination
239 of the saturation time, t_{plateau} , viz inflection point of the breakthrough curves, was determined using
240 the 1st derivative of the UV-signal. For each ligand concentration, $[L]$, the breakthrough curve is used
241 to determine the amount of ligand captured by the HSA affinity support, q , using eq. 1:

242

$$243 \quad q = \Delta t \times F \times [L] \quad (\text{Eq.1})$$

244

245 Δt being the time difference between dead time, t_0 , and saturation time, t_{plateau} .

246 The total number of active sites on the affinity column, B_{act} , and the dissociation equilibrium
247 constant, K_d , of the HSA-ligand complex were determined according to eq. 2 after plotting $1/q$ versus
248 $1/[L]$:

249

$$250 \quad \frac{1}{q} = \frac{k_d}{B_{act}} \times \frac{1}{[L]} + \frac{1}{B_{act}} \quad (\text{Eq.2})$$

251

252 B_{act} was first determined in pmol and then converted to pmol.cm^{-1} and nmol.mL^{-1} using the monolith
253 density (300 and 320 mg.mL^{-1} respectively for silica and organic monolith).

254 **2.5.2 Evaluation of non-specific interactions**

255 Non-specific interactions were quantified by frontal analysis using a ligand concentration of $10 \mu\text{M}$ in
256 phosphate buffer ($67 \text{ mM K}_2\text{HPO}_4$, pH 7.4) on monolithic columns before the protein immobilization
257 step. For each support, the amount of probe ligands captured by non-specific interaction was
258 determined according to Eq.1. For non-specific interactions, the breakthrough volume is the same at
259 all concentrations and the amount of ligand captured is directly proportional to the concentration.
260 The contribution of non-specific interactions to total retention was also expressed as the fraction of
261 ligand captured by non-specific interactions compared to the total amount captured by frontal
262 affinity chromatography on the same monolith after the protein immobilization step (at the same
263 ligand concentration).

264 **2.5.3 Determination of the total amount of immobilized protein B_{tot}**

265 In order to thoroughly characterize the influence of the immobilization process on the protein
266 activity, the active amount of HSA, B_{act} , has to be compared to the total amount of immobilized
267 protein, B_{tot} . So different methods were designed to determine *in-situ* the total amount of target
268 protein immobilized according to the protein grafting process.

269

270 For monoliths bio-functionalized with the streptavidin-biotin coupling method, the UV-monitoring of
271 the breakthrough curve of biotin-HSA at 230 and 280 nm during the dynamic grafting step allowed
272 the direct quantification of biotin-HSA captured by the monolith.

273

274 For affinity monoliths prepared with the Schiff base method, the Amino Density Estimation by
275 Colorimetric Assay (ADECA) method was adapted to micro-format and hydrodynamic mode from
276 results previously obtained in a static mode on macro-monoliths synthesized in batch [25]. The on-
277 line modified ADECA method use the Coomassie Brilliant Blue (CBB) dye and allows for *in-situ*
278 determinations of the total amount of protein grafted inside miniaturized capillary column,

279 independently of its activity. The experiments were conducted using the CE system in the short-end
280 injection mode using external pressuring device. The monolith is initially flushed with ultrapure water
281 to remove the phosphate buffer, and a 10% methanol-5% acetic acid solution to protonate all amino
282 groups, both at 1.2 MPa for 10 min. Then, a 100 mg.L⁻¹ CBB in 10 % v/v methanol-5 % v/v acetic acid
283 solution is loaded under a 1.2 MPa pressure monitoring the corresponding breakthrough curve at
284 260 nm. Eq. 1 was used to determine the amount of captured CBB and the quantity of immobilized
285 protein was calculated taking into account the 103 amino acids, distributed between lysine, histidine
286 and arginine, in the HSA sequence. The rinsing step was performed by flushing the column with a
287 50/50 1 M ammonia/methanol solution at 1.2 MPa for 10 min.
288

289 **3. Results and discussion**

290 Two types of monolithic capillary supports were investigated for the development of miniaturized
291 weak affinity experiments: silica and organic monoliths. Both types were first *in-situ* synthesized in
292 75 µm i.d. capillary and then bio-functionalized with HSA as model target protein. Depending on the
293 type of monolith, several bio-functionalization pathways were considered: the direct “epoxy” and
294 “Schiff base” methods and the “streptavidin-biotin” coupling method (Fig. 2).

295 Fig.2.
296

297 For the streptavidin-biotin coupling method described in this paper, streptavidin was grafted on the
298 surface and biotin was attached to HSA. Then, due to the rapid and complete streptavidin-biotin
299 interaction, the capture of the biotin-protein was monitored *in-situ* by UV spectrophotometry during
300 its breakthrough percolation.

301

302 The HSA immobilized organic and silica monoliths were evaluated in terms of unwanted non-specific
303 interactions and specific interactions (affinity), with the goal to minimize the former and to enhance
304 the latter. Considering the high permeability of monoliths, the use of an expensive nano-LC set-up
305 was put aside and all experiments were conducted in frontal affinity chromatography using a
306 capillary electrophoresis system, operated in the pressurized mode (maximum external pressure of
307 1.2 MPa) in the short-end mode.

308

309 **3.1. Affinity Silica monoliths**

310 A first attempt to downsize weak affinity chromatography at nanoscale was made with silica
311 monoliths that present similar chemical and textural features to that of silica particles used in the

312 literature. Bare silica monoliths were *in-situ* synthesized according to a previously described sol-gel
313 protocol [21]. Such monolithic capillary columns have 2 μm through-pores with 8 nm mesopores
314 giving a surface area of $480 \text{ m}^2 \cdot \text{g}^{-1}$ with a 1.5 μm skeleton diameter giving a permeability of $5 \cdot 10^{-14} \text{ m}^2$
315 (determined by Darcy's law). For comparison, classical 3-5 μm silica particles have larger mesopores,
316 specific areas between 100 and $300 \text{ m}^2 \cdot \text{g}^{-1}$, and permeabilities two orders of magnitude lower.

317

318 Only the two direct epoxy-amine and the Schiff base bio-functionalization processes of Fig. 2 were
319 initially considered with silica monolithic columns. Indeed, the streptavidin-biotin coupling is not
320 amenable with 8 nm nanopores. Bare silica monoliths were silanized with
321 glycidoxypropyltrimethoxysilane (GPTMS) leading to epoxy-functionalized silica monoliths. Epoxy-
322 ring opening was achieved in acidic medium to form diol groups that were oxidized into aldehyde
323 groups. The silica monoliths were evaluated at different stages of modification in terms of non-
324 specific and specific affinity interactions.

325

326 **3.1.1 Non-specific interactions on silica monoliths.**

327 Characterization of non-specific interactions was estimated through adsorption of three HSA-specific
328 ligands: warfarin, furosemide and ibuprofen, at a unique concentration of 10 μM . Their adsorption
329 on silica monolith surfaces was done at four different stages of modification: (i) bare silica monolith,
330 (ii) epoxy-modified silica monolith, (iii) diol monolith after the epoxy-ring opening, and (iv) reduced-
331 aldehyde monolith. Fig. 3 shows the absorbed amounts of three ligands on the 8.5 cm effective
332 length 75 μm i.d. capillaries, expressed in $\text{pmol} \cdot \text{cm}^{-1}$, obtained on bare monolith and at the different
333 stages of modification. The epoxy-activated silica monoliths present the highest level of non-specific
334 interactions, probably linked to the less hydrophilic character of the glycidoxypropyl group
335 introduced during the silanization step. Hydrolysis of the epoxy-ring into diol groups significantly
336 decreases the amount of non-specifically adsorbed ligands but the level remains twice higher than on
337 bare silica (Fig. 3). The oxidation of the diol moieties into aldehydes, followed by their reduction by
338 NaBH_4 to polar hydroxyl groups does not significantly decrease non-specific interactions.

339

Fig.3.

340

341 Since the log D values at pH=7.4 of these three negatively charged ligands, respectively around -1, 0.8
342 and 1 for furosemide, warfarin and ibuprofen [26], do not match the non-specific interaction levels,
343 hydrophobicity is not the only contributing factor. This significant level highlights that non-specific
344 interactions should not be neglected on silica affinity monoliths and that reference columns have to
345 be prepared to quantify their contribution to overall retention. When the Schiff base method is used,
346 diol columns can be used instead of a reduced-aldehyde ones as non-specific interactions are of the

347 same order of magnitude for both column types (Fig. 3). Diol columns are easier-to-synthesize
 348 references. If such a strategy, evaluation of non-specific interactions without any protein
 349 immobilized onto the surface, is usually recommended by several groups (Hage, Ohlson) it may not
 350 be fully representative of the final affinity column. Indeed, once proteins are grafted onto the
 351 support, the resulting surface is partially covered by the targets, thus probably limiting ligand
 352 accessibility to the underlying support. However, the grafting of another protein is not a satisfactory
 353 alternative as it may lead itself to other non-specific interactions (from electrostatic to hydrophobic
 354 ones).

355

356 **3.1.2 Affinity on HSA-silica monoliths.**

357 The epoxy-method is known to proceed through the quick adsorption of the protein onto the surface
 358 followed by a slower covalent links formation between epoxy and amino residues of biomolecules
 359 [27]. Adsorption of a protein onto a hydrophobic surface is known to partially denature it i.e. to alter
 360 its biological activity [28]. Thus the epoxy method was not further investigated on the epoxy silica
 361 and HSA-affinity silica monolithic columns were exclusively prepared through the Schiff base method.
 362 The performances of these affinity columns were assessed in frontal affinity chromatography (FAC)
 363 with the three ligands. These ligands target the two main interaction sites of HSA (Sudlow sites IIA
 364 and IIIA) [6,11]. For each solute, the breakthrough volume increased when the infused concentration
 365 decreased, which is characteristic of affinity. Both the experimental K_d values and the total amount of
 366 active binding sites (B_{act}) of immobilized target proteins were determined by plotting the reciprocal
 367 of the amount of captured ligand ($1/q$) versus the reciprocal of the ligand concentration ($1/[L]$) (Eq.
 368 2). The values are reported in Table 1.

369

Grafting method	Columns tested	Binding site	Compound	K_d in literature (μM)	Calculated K_d (μM)	Active HSA content (B_{act})	
						($\text{pmol}\cdot\text{cm}^{-1}$)	($\text{nmol}\cdot\text{mL}^{-1}$)
Schiff base	n=3	IIA	Warfarin	2 – 7	20 \pm 8	10 \pm 2	212 \pm 47
			Furosemide	5 – 50	97 \pm 36	32 \pm 7	680 \pm 150
		IIIA	Ibuprofen	0.3 – 25	116 \pm 43	32 \pm 7	680 \pm 150

370 **Table 1.** Experimental K_d values and active HSA-content for silica monoliths bio-functionalized
 371 with HSA via the Schiff base method. Frontal analysis experiments implemented on silica
 372 monolithic columns (effective length = 8.5 cm, 75 μm i.d.). Relative standard deviations for the
 373 three experiments.

374

375 The fact that the three ligands exhibit a measurable affinity for the HSA-column indicates that the
 376 two HSA binding sites are active. However, the experimental K_d values obtained in this work (Table 1)
 377 are slightly higher than those reported in the literature [24] (Fig. 1). The high surface area of the silica

378 monolith ($480 \text{ m}^2 \cdot \text{g}^{-1}$) did not produce a higher number active sites B_{act} compared to the number of
379 sites found on silica particles with only $100 \text{ m}^2 \cdot \text{g}^{-1}$ [15]. The relative small size of the monolith
380 mesopores (8 nm) combined to the high total monolith porosity may account for this relatively low
381 active site density. The native HSA protein is quite large with a hydrodynamic radius of 3.5 nm likely
382 to produce steric hindrances in mesopores that make most of the surface area. In addition, the small
383 phase ratio V_s/V_m of silica monoliths, that are about 90 % porous, is less favorable to binding than
384 that of silica particles with only 70-80 % total porosity.

385 Considering the relative amounts of solutes captured at the same concentration (10 μM
386 concentration) on the HSA-silica monoliths and on reduced-aldehyde monoliths, non-specific
387 interactions make a substantial contribution to the overall retention (respectively 7%, 18% and 41%
388 for ibuprofen, furosemide and warfarin at 10 μM). This level of non-specific interactions to overall
389 retention is similar to what was observed by several authors on silica particles [15]. The difference in
390 active HSA-content (B_{act}) obtained for the same IIA binding site with two different ligands (Table 1)
391 suggests that these values could be partially biased by non-specific interactions that are more
392 important for warfarin. Considering (i) the relatively high part of non-specific interactions and (ii) the
393 impossibility to enlarge the mesopore diameter of our silica monoliths to increase access to the pore
394 volume, further investigation was focused on organic monoliths.

395

396 **3.2. Glycidyl methacrylate affinity monoliths**

397 Among the great diversity of organic monoliths [18], the GMA ones were selected for the simplicity
398 and rapidity of their photochemically induced synthesis leaving directly available epoxy reactive
399 groups at their surface. They were *in-situ* synthesized in UV-transparent capillaries according to a
400 described protocol [22]. UV-masks allow for an easy selection of monolith length and location in the
401 capillary. This monolith had a specific area of $4 \text{ m}^2 \cdot \text{g}^{-1}$ and a permeability of 10^{-13} m^2 .

402 All the protein immobilization pathways described in Fig. 2 were possible with the GMA monoliths.
403 The systematic non-specific interaction study was done in order to estimate the benefits of each
404 pathway with respect to affinity measurement on GMA-based monolith.

405

406 **3.2.1 Non-specific interactions on organic GMA monoliths**

407 Possible non-specific interactions were investigated at the different stages of the monolith
408 elaboration: (i) as-synthesized, (ii) after the epoxy-ring opening to form diols, (iii) after diol oxidation
409 into aldehyde and reduction of the aldehyde with NaBH_4 , and (iv) after the covalent grafting of
410 streptavidin. Fig. 4 presents the non-specific adsorption of the three ligands at each step.

411

412 The highest adsorption value in Fig. 4 ($0.43 \text{ pmol.cm}^{-1}$) is lower than the adsorption values on silica
 413 monolith (Fig. 3). Clearly, organic monoliths, at all elaboration stages, show less non-specific
 414 interactions than silica monoliths. The dramatically lower amounts of ligands adsorbed onto GMA
 415 and GMA-modified monoliths compared to silica monoliths may be due to the much lower surface
 416 area of the organic monoliths. Among the GMA-based monoliths, epoxy monolith exhibits the
 417 highest level of non-specific interactions. As expected, the conversion of epoxy into diol groups led to
 418 a significant decrease in non-specific interactions that remain quite identical after oxidation. (Fig. 4).
 419 After the grafting of streptavidin, the level of non-specific interaction slightly increases, thus
 420 demonstrating that the grafting of a protein onto the surface is not a better alternative to hide the
 421 underlying surface and may lead to small non-specific interactions.

422

423 3.2.2 Affinity on GMA-based monoliths

424 Frontal affinity chromatography was used to characterize the immobilized-HSA activity and
 425 accessibility with respect to the three HSA immobilization pathways. The K_d values and amount of
 426 active binding sites B_{act} are gathered in Table 2. An illustration of the affinity experiments conducted
 427 on a streptavidin-biotin monolith (breakthrough curves and plot of $1/q$ vs $1/[L]$) is given in S.2. For
 428 HSA-columns prepared through the Schiff base and streptavidin-biotin methods, the total HSA
 429 content was *in-situ* determined. The colorimetric ADECA method was implemented to quantify the
 430 total amount (B_{tot}) of HSA immobilized onto the aldehyde monolith via the Schiff base method. The
 431 total amount of biotin-HSA captured on the streptavidin-column was directly quantified through the
 432 breakthrough curves (S.2). The ratio between active and total HSA contents gives the HSA activity
 433 yield.

434

Grafting method	Columns tested	Binding site	Compound	Calculated K_d (μM)	Active HSA content (B_{act})		Total HSA content (B_{tot})		Activity yield
					(pmol.cm^{-1})	(nmol.mL^{-1})	(pmol.cm^{-1})	(nmol.mL^{-1})	
Epoxy	n=3	IIA	Warfarin	17 ± 9	5 ± 1	103 ± 27	Not determined (high non-specific interactions)		
			Furosemide	24 ± 13	4.0 ± 0.8	91 ± 24			
		IIIA	Ibuprofen	21 ± 11	2.6 ± 0.5	59 ± 15			
Schiff base	n=13	IIA	Warfarin	11 ± 5	1.9 ± 0.5	43 ± 11	2.4 ± 0.8	54 ± 18	71%
			Furosemide	17 ± 3	1.7 ± 0.6	38 ± 14			
		IIIA	Ibuprofen	12 ± 1	1.5 ± 0.4	34 ± 9			
Streptavidin	n=13	IIA	Warfarin	13 ± 4	4 ± 1	91 ± 22	4.9 ± 0.6	111 ± 14	84%
			Furosemide	18 ± 7	4.2 ± 0.8	95 ± 18			
		IIIA	Ibuprofen	16 ± 4	4.0 ± 0.5	91 ± 12			

435 **Table 2.** Experimental K_d values, active HSA-content (B_{act}) and total HSA-content (B_{tot}) for GMA-
 436 based monoliths bio-functionalized with HSA via different immobilization pathways. Frontal

437 analysis experiments implemented on monolithic columns (effective length = 8.5 cm, 75 μm i.d.).
438 Relative standard deviations for the n experiments.
439

440 The K_d values obtained for the three test ligands are in good agreement with previously reported
441 values and show that the two binding sites of immobilized HSA are active whatever the grafting
442 method used.

443 Another important point is the relative amount of ligand captured by non-specific versus that
444 captured by specific interactions. The level of non-specific interactions (at 10 μM) ranges from 16 to
445 34 % (epoxy), 0 to 8 % (Schiff base) and 0 to 7 % (streptavidin monoliths). These results show that
446 GMA-modified monoliths present a significantly lower contribution of non-specific interaction than
447 their silica counterparts.
448

449 3.2.2.1 Epoxy method

450 Regarding the active sites content (B_{act}), different values were obtained for the two HSA binding sites.
451 Whereas about 4-5 $\text{pmol}\cdot\text{cm}^{-1}$ of active sites is measured on the site IIA, only about 2.5 $\text{pmol}\cdot\text{cm}^{-1}$ of
452 active sites is afforded for the site IIIA (n=3) (Table 2). This difference may be partially ascribe to
453 non-specific interactions on the epoxy-monolith and/or to a partial loss of activity of the Sudlow site
454 IIIA consecutive to the HSA immobilization process as already observed on silica [9]. Several attempts
455 were made to reduce or suppress non-specific interactions on epoxy monoliths using different post-
456 grafting reactions. Post-grafting modification proposed in the literature were tested unsuccessfully:
457 the monoliths were treated with tris(hydroxymethyl)-aminomethane (Tris) (0.1 M, pH 8.6, 48 h),
458 cysteine (1 M, 48 h), or ethanolamine (1 M, 15 h) [7,16]. FTIR spectroscopy was used to follow the
459 reaction of epoxy groups. No reduction of the intensity of the C-O vibration band of the epoxy at 907
460 cm^{-1} was observed, which confirms the lack of reactivity of Tris and ethanolamine at room
461 temperature. Increasing the temperature to 60°C was effective in opening the epoxy groups but it
462 was not practical due to obvious protein stability issues. Conversely, the reaction of epoxy groups
463 with cysteine was efficient by totally eliminating non-specific interactions at room temperature, but
464 it also suppressed all HSA-specific interactions with the ligands. According to the literature, cysteine
465 may form a disulfide bond with the free ³⁴Cysteine of HSA impairing all activity of the binding sites by
466 oxidation cascade [29]. Despite the simplicity of the direct grafting of HSA onto poly(GMA-co-EDMA)
467 monoliths, this modification pathway was no further investigated due to excessive non-specific
468 interactions and potential partial deactivation of site IIIA.
469

470 3.2.2.2 Schiff base and streptavidin-biotin method

471 Very coherent active sites B_{act} were obtained with the three ligands on affinity monoliths prepared by
472 immobilization of HSA using the Schiff base method or the streptavidin-biotin coupling (Table 2). This
473 accurate determination of B_{act} is probably related to the very low level of non-specific interactions (in
474 the low percent range). Also, the concordant values obtained for the two sites indicate that no partial
475 deactivation of the IIIA site occurs with these two bio-functionalization methods. This outlines the
476 proper accessibility of immobilized proteins with equivalent activities for the two binding sites (IIA
477 and IIIA).

478

479 There is more than twice less HSA on the Schiff base monoliths *viz* 1.7 pmol.cm^{-1} ($n=13$) compared to
480 the streptavidin-biotin one with 4 pmol.cm^{-1} ($n=13$) (Table 2). Also, the amount of active HSA, ratio
481 (B_{act})/ (B_{tot}) is 84% for the streptavidin monolith, slightly better than the 71% for the Schiff base
482 monoliths. Assuming that reduced-aldehyde monoliths bind the same amount of streptavidin than of
483 HSA (these two proteins have similar features in terms of mass, hydrophobicity and isoelectric point),
484 it was estimated that one tetramer of streptavidin binds to two biotin-HSA.

485

486 **3.2.3 Grafting duration and protein consumption considerations**

487 Optimization of the protein immobilization concerns the reaction time and the quantity of target
488 protein used for the immobilization step. In the literature, grafting durations with the Schiff base
489 method range from 3 to 6 days (0.5 mL.min^{-1}) for HSA concentrations of 5 mg.mL^{-1} [6,7,16]. Our
490 protocol uses a twice to ten times less concentrated HSA solution (2 down to 0.5 mg.mL^{-1}) and the
491 grafting time is six to ten times faster completed in 48h then downed to 12 h in dynamic mode at a
492 linear velocity of about 0.06 cm.s^{-1} . No significant difference in active HSA content was observed
493 between the different columns, validating the grafting under flow conditions (dynamic mode) [4,9].
494 Another real advantage, beside time and protein mass savings, is the greatly reduced risk of loss of
495 protein activity and/or denaturation.

496 The streptavidin-biotin coupling process is faster than the two other modes which is a great
497 advantage with proteins of low stability. The coupling of biotinylated-target protein can be achieved
498 in few minutes, e.g. about 15 min with a 1 mg.mL^{-1} protein concentration and a 8.5 cm effective
499 length $75 \text{ }\mu\text{m}$ i.d. column at a percolation pressure of 1.2 MPa. This coupling can be applied just
500 before the affinity experiments: the column is installed in the CE cartridge, grafted in dynamic mode
501 (under UV monitoring) and ready to use. Last but not least, the UV monitoring during the grafting
502 step of the biotin-protein onto the streptavidin support allows for (i) minimizing the protein
503 consumption to a few pmol per centimeter of capillary column, and (ii) the exact determination of

504 the amount of grafted protein which is a tremendous asset for the quality control of each column
505 before its use.

506

507 **3.2.4 Stability of the streptavidin-biotin affinity columns**

508 Stability of the bio-functionalized columns is of great concern. Indeed, screening affinity of unknown
509 ligands against a specific target protein implies preserving the protein activity during the screening
510 process as well as the protein content constant during successive analyses. Long-term stability and
511 storage conditions must be also examined.

512 *3.2.4.1 Stability of streptavidin-functionalized monolithic columns*

513 The stability of streptavidin-functionalized columns was not considered so far. So, it was checked if it
514 is possible to prepare and to stock streptavidin-functionalized columns for a long time at 4°C before
515 their coupling with the biotinylated-target protein.

516 Six streptavidin-functionalized columns synthesized through the Schiff base method were prepared.
517 Three were coupled with biotin-HSA and used immediately. The other three were stored at 4°C for
518 three months. The columns stored at 4°C kept their trapping ability intact as per biotin-HSA content
519 after 3 months. Thus, the streptavidin-functionalized columns can be prepared in advance and stored
520 for at least three months before use, knowing that protein coupling is rapid and easy and can be
521 done freshly before the affinity study.

522 *3.2.4.2 Stability of affinity-HSA columns (prepared by the streptavidin-biotin coupling)*

523 The stability of HSA-affinity columns may be a critical parameter especially in the case of a screening
524 campaign as it will determine the useful lifetime of the column. The stability of the HSA affinity
525 columns was evaluated in phosphate buffer (67 mM, pH=7.4) using frontal analysis with warfarin to
526 determine the remaining amount of active protein (B_{act}) under various temperature conditions,
527 namely: (i) at 4°C i.e. in storage conditions, (ii) at room temperature in static mode and (iii) at room
528 temperature in dynamic mode (screening conditions).

529

530 At 4°C, no variation of the active HSA content (B_{act}) was observed within 3 months, thus indicating
531 that affinity columns can be prepared in advance and used later. At room temperature and in
532 dynamic conditions, the column being continuously flushed with buffer at $0.06 \text{ cm}\cdot\text{s}^{-1}$, 80% of active
533 HSA were remaining after 24 hours and around 550 column volumes. 64% remained after 80 hours of
534 extensive use or over 1800 column volumes. In order to assess if the partial loss of activity was due
535 to protein stability or to the sustained released of poorly or unbound HSA, the same experiment was
536 carried out in static mode. After 80 h of storage at room temperature in static mode, the remaining

537 activity was only 55%. This result indicates that exposure to room temperature is responsible for the
538 loss of activity and that there is no loss of protein by leaching.

539

540 **3.3. HSP90 affinity columns**

541 As HSA affinity columns gave promising results with organic monolith grafted by the streptavidin-
542 biotin approach, affinity columns were then prepared by the same method with another soluble
543 protein: the N-terminal domain of HSP90. Grafted quantity of HSP90 ($5.8 \pm 0.7 \text{ pmol.cm}^{-1}$, $n=11$
544 columns) is similar to HSA ($4.9 \pm 0.6 \text{ pmol.cm}^{-1}$, Table 2). Two known ligands were studied by frontal
545 affinity chromatography to validate the technique on a different protein: adenosine diphosphate
546 (ADP, $K_d=10\text{-}15 \text{ }\mu\text{M}$ [30]) and *n,n*-diethylvanillamide ($K_d=790 \text{ }\mu\text{M}$ [30]). Specific interactions were
547 detected for both ligands and calculated dissociation constants ($14 \pm 2 \text{ }\mu\text{M}$ and $150 \pm 70 \text{ }\mu\text{M}$
548 respectively for ADP and *n,n*-diethylvanillamide) were in the literature range. It may be noted that
549 the weaker the affinity, the higher the uncertainty on K_d determination. Specific affinity was also
550 detected for a third ligand, 3-hydroxy-4-methoxybenzyl alcohol and the affinity was estimated at
551 about $40 \text{ }\mu\text{M}$ (no reference K_d was found in the literature). It seems therefore possible to graft
552 different proteins with the streptavidin-biotin approach while maintaining their specific binding
553 capacity.

554

555 **4. Conclusion**

556 Results obtained during this evaluation of two types of monoliths, a silica based and an organic
557 glycidyl methacrylate based one, and different ways of protein grafting led us to the following
558 conclusions: silica based monoliths can load a higher amount of active protein, but a high level of
559 non-specific interactions is noted when interacting with ligands. The silica grafting of reactive
560 moieties requires a first step that is silanization with glycidoxypropyltrimethoxysilane. It is thought
561 that this silanization step is responsible, at least partly, for the non-specific interactions. Non-specific
562 hydrophobic interactions with the propyl linker are possible. Due to a higher adsorption and a lower
563 permeability on silica monoliths, it seems better for our purpose to work with GMA monoliths.

564 GMA monoliths may be directly grafted with proteins. However, some residual epoxy moieties are
565 left over after target grafting. These reactive epoxy groups cannot be efficiently suppressed under
566 reaction conditions compatible with the grafted protein stability. Protein grafting using the Schiff
567 base method or the streptavidin-biotin method produced the best organic monoliths: negligible non-
568 specific interactions and high active protein content. The very low protein consumption is another
569 significant advantage for the streptavidin-biotin method.

570 The method requires a first step that is attaching biotin to the target protein, which is
571 straightforward. This said the method presents several advantages over the Schiff base method: (i) it
572 binds up to twice more active sites allowing targeting lower affinity ligands. (ii) The streptavidin
573 column can be loaded in a few minutes with the target protein just prior its use thus limiting stability
574 issues. (iii) For each column, the exact amount of biotinylated-target protein captured during the
575 grafting step is exactly known, which is a major asset for quality control. (iv) The amount of bound
576 protein (a few ten picomoles per column) is just what is needed. (v) The method does not denature
577 the protein giving an activity rate passing 80%. Such streptavidin-biotin grafting way is generic, as it
578 may be implemented to any other biotinylated target. Indeed, it has been shown that this method
579 was successfully applied to the N-terminal domain of HSP90.

580 As an example of the benefits of 8.5 cm effective length 75 μm i.d. miniaturized monolith columns
581 modified by the streptavidin-biotin method, the grafting requires only 40 pmol of the target protein
582 (3 μg for a 70 kDa protein). It is achieved in about 10 min with a pressure drop of 1.2 MPa giving a
583 flow rate of 240 $\text{nL}\cdot\text{min}^{-1}$ and a 1 $\text{mg}\cdot\text{mL}^{-1}$ protein concentration. The great monolith permeability of
584 these nano-columns can be operated in a very simple and automated way with the external pressure
585 device of a common capillary electrophoresis system using its in-situ UV detection avoiding all nano-
586 LC problems with high pressure particle-filled columns.

587 In the frame of screening process (using zonal affinity chromatography analysis coupled to mass
588 spectrometry), it will be possible to screen mixtures of about 10-20 compounds in one analysis of
589 about 30 min, which gives around 48 runs/day i.e. around 500-1000 compounds/day (namely an
590 entire fragment library in the fragment-based drug discovery (FDBB) approach). Thus, boosting the
591 fragment screening step using a generic method (applicable to any biotinylated proteins) is of great
592 interest in FBDD.

593

594 **Funding**

595 This work was partially funded by Servier laboratories.

596

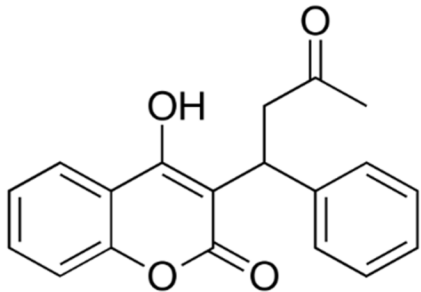
597 **References**

598

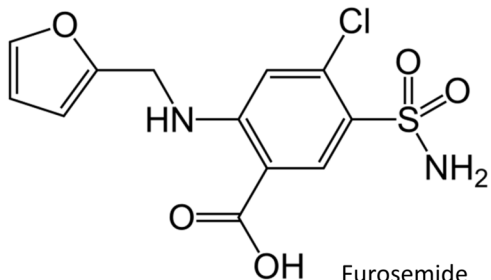
599 [1] Hans-Joachim Böhm, Gisbert Schneider, Raimund Mannhold, Hugo Kubinyi, Gerd Folkers,
600 Protein-Ligand Interactions: From Molecular Recognition to Drug Design, Wiley-VCH, H.-J.
601 Böhm and G. Schneider, Weinheim, 2003.

- 602 [2] N.W.C. Chan, D.F. Lewis, P.J. Rosner, M.A. Kelly, D.C. Schriemer, Frontal affinity
603 chromatography–mass spectrometry assay technology for multiple stages of drug discovery:
604 applications of a chromatographic biosensor, *Anal. Biochem.* 319 (2003) 1–12.
605 doi:10.1016/S0003-2697(03)00193-3.
- 606 [3] E. Meiby, H. Simmonite, L. le Strat, B. Davis, N. Matassova, J.D. Moore, M. Mrosek, J. Murray,
607 R.E. Hubbard, S. Ohlson, Fragment screening by weak affinity chromatography: comparison
608 with established techniques for screening against HSP90, *Anal. Chem.* 85 (2013) 6756–6766.
609 doi:10.1021/ac400715t.
- 610 [4] M.J. Yoo, J.E. Schiel, D.S. Hage, Evaluation of affinity microcolumns containing human serum
611 albumin for rapid analysis of drug–protein binding, *J. Chromatogr. B.* 878 (2010) 1707–1713.
612 doi:10.1016/j.jchromb.2010.04.028.
- 613 [5] S. Ohlson, M.-D. Duong-Thi, Fragment screening for drug leads by weak affinity
614 chromatography (WAC-MS), *Methods.* (2018). doi:10.1016/j.ymeth.2018.01.011.
- 615 [6] R. Mallik, D.S. Hage, Development of an affinity silica monolith containing human serum
616 albumin for chiral separations, *J. Pharm. Biomed. Anal.* 46 (2008) 820–830.
617 doi:10.1016/j.jpba.2007.03.017.
- 618 [7] E.L. Pfaunmiller, M. Hartmann, C.M. Dupper, S. Soman, D.S. Hage, Optimization of human
619 serum albumin monoliths for chiral separations and high-performance affinity chromatography,
620 *J. Chromatogr. A.* 1269 (2012) 198–207. doi:10.1016/j.chroma.2012.09.009.
- 621 [8] M.L. Conrad, A.C. Moser, D.S. Hage, Evaluation of indole-based probes for high-throughput
622 screening of drug binding to human serum albumin: analysis by high-performance affinity
623 chromatography, *J. Sep. Sci.* 32 (2009) 1145–1155. doi:10.1002/jssc.200800567.
- 624 [9] B. Loun, D.S. Hage, Characterization of thyroxine—albumin binding using high-performance
625 affinity chromatography, *J. Chromatogr. B. Biomed. Sci. App.* 579 (1992) 225–235.
626 doi:10.1016/0378-4347(92)80386-5.
- 627 [10] Y. Liang, J. Wang, F. Fei, H. Sun, T. Liu, Q. Li, X. Zhao, X. Zheng, Binding kinetics of five drugs to
628 beta2-adrenoceptor using peak profiling method and nonlinear chromatography, *J.*
629 *Chromatogr. A.* 1538 (2018) 17–24. doi:10.1016/j.chroma.2018.01.027.
- 630 [11] K.S. Joseph, A.C. Moser, S. Basiaga, J.E. Schiel, D.S. Hage, Evaluation of alternatives to warfarin
631 as probes for sudlow site I of human serum albumin characterization by high-performance
632 affinity chromatography, *J. Chromatogr. A.* 1216 (2009) 3492–3500.
633 doi:10.1016/j.chroma.2008.09.080.
- 634 [12] X. Zheng, M. Podariu, C. Bi, D.S. Hage, Development of enhanced capacity affinity
635 microcolumns by using a hybrid of protein cross-linking/modification and immobilization, *J.*
636 *Chromatogr. A.* 1400 (2015) 82–90. doi:10.1016/j.chroma.2015.04.051.
- 637 [13] R. Matsuda, J. Anguizola, K.S. Hoy, D.S. Hage, Analysis of drug-protein interactions by high-
638 performance affinity chromatography: interactions of sulfonylurea drugs with normal and
639 glycosylated human serum albumin, *Methods Mol. Biol. Clifton NJ.* 1286 (2015) 255–277.
640 doi:10.1007/978-1-4939-2447-9_21.
- 641 [14] M. Strandh, H.S. Andersson, S. Ohlson, Weak Affinity Chromatography, in: *Affin. Chromatogr.*,
642 Humana Press, New Jersey, 2000: pp. 7–23. doi:10.1385/1-59259-041-1:7.
- 643 [15] M.J. Yoo, D.S. Hage, Evaluation of silica monoliths in affinity microcolumns for high-throughput
644 analysis of drug-protein interactions, *J. Sep. Sci.* 32 (2009) 2776–2785.
645 doi:10.1002/jssc.200900346.
- 646 [16] R. Mallik, T. Jiang, D.S. Hage, High-performance affinity monolith chromatography:
647 development and evaluation of human serum albumin columns, *Anal. Chem.* 76 (2004) 7013–
648 7022. doi:10.1021/ac049001q.
- 649 [17] M.-D. Duong-Thi, M. Bergström, T. Fex, S. Svensson, S. Ohlson, R. Isaksson, Weak affinity
650 chromatography for evaluation of stereoisomers in early drug discovery, *J. Biomol. Screen.* 18
651 (2013) 748–755. doi:10.1177/1087057113480391.

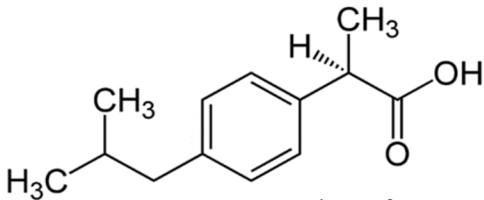
- 652 [18] C. Acquah, C.K.S. Moy, M.K. Danquah, C.M. Ongkudon, Development and characteristics of
653 polymer monoliths for advanced LC bioscreening applications: A review, *J. Chromatogr. B.*
654 1015–1016 (2016) 121–134. doi:10.1016/j.jchromb.2016.02.016.
- 655 [19] H.S. Kim, R. Mallik, D.S. Hage, Chromatographic analysis of carbamazepine binding to human
656 serum albumin, *J. Chromatogr. B.* 837 (2006) 138–146. doi:10.1016/j.jchromb.2006.03.062.
- 657 [20] M. Ozawa, T. Ozawa, M. Nishio, K. Ueda, The role of CH/ π interactions in the high affinity
658 binding of streptavidin and biotin, *J. Mol. Graph. Model.* 75 (2017) 117–124.
659 doi:10.1016/j.jmglm.2017.05.002.
- 660 [21] R. El Debs, V. Dugas, C. Demesmay, Photografting as a versatile, localizable, and single-step
661 surface functionalization of silica-based monoliths dedicated to microscale separation
662 techniques., *J. Sep. Sci.* 36 (2013) 993–1001. doi:10.1002/jssc.201200878.
- 663 [22] A. Bruchet, V. Dugas, C. Mariet, F. Goutelard, J. Randon, Improved chromatographic
664 performances of glycidyl methacrylate anion-exchange monolith for fast nano-ion exchange
665 chromatography, *J. Sep. Sci.* 34 (2011) 2079–2087. doi:10.1002/jssc.201100180.
- 666 [23] G.T. Hermanson, Chapter 11 - (Strept)avidin–Biotin Systems, in: G.T. Hermanson (Ed.),
667 *Bioconjugate Tech. Third Ed.*, Academic Press, Boston, 2013: pp. 465–505. doi:10.1016/B978-0-
668 12-382239-0.00011-X.
- 669 [24] M.D. Shorridge, D.S. Hage, G.S. Harbison, R. Powers, Estimating protein-ligand binding affinity
670 using high-throughput screening by NMR, *J. Comb. Chem.* 10 (2008) 948–958.
671 doi:10.1021/cc800122m.
- 672 [25] C. Faye, J. Chamieh, T. Moreau, F. Garnier, K. Faure, V. Dugas, C. Demesmay, O. Vandenneele-
673 Trambouze, In situ characterization of antibody grafting on porous monolithic supports, *Anal.*
674 *Biochem.* 420 (2012) 147–154. doi:10.1016/j.ab.2011.09.016.
- 675 [26] Y.W. Alelyunas, L. Pelosi-Kilby, P. Turcotte, M.-B. Kary, R.C. Spreen, A high throughput dried
676 DMSO LogD lipophilicity measurement based on 96-well shake-flask and atmospheric pressure
677 photoionization mass spectrometry detection, *J. Chromatogr. A.* 1217 (2010) 1950–1955.
678 doi:10.1016/j.chroma.2010.01.071.
- 679 [27] C. Mateo, V. Grazú, B.C.C. Pessela, T. Montes, J.M. Palomo, R. Torres, F. López-Gallego, R.
680 Fernández-Lafuente, J.M. Guisán, Advances in the design of new epoxy supports for enzyme
681 immobilization–stabilization, *Biochem. Soc. Trans.* 35 (2007) 1593–1601.
682 doi:10.1042/BST0351593.
- 683 [28] J.E. Butler, Solid Supports in Enzyme-Linked Immunosorbent Assay and Other Solid-Phase
684 Immunoassays, *Methods.* 22 (2000) 4–23. doi:10.1006/meth.2000.1031.
- 685 [29] K. Oettl, R.E. Stauber, Physiological and pathological changes in the redox state of human
686 serum albumin critically influence its binding properties, *Br. J. Pharmacol.* 151 (2007) 580–590.
687 doi:10.1038/sj.bjp.0707251.
- 688 [30] R. Buratto, D. Mammoli, E. Chiarparin, G. Williams, G. Bodenhausen, Exploring weak ligand–
689 protein interactions by long-lived NMR states: improved contrast in fragment-based drug
690 screening, *Angew. Chem. Int. Ed Engl.* 53 (2014) 11376–11380. doi:10.1002/anie.201404921.
- 691



Warfarin
Site IIA
 $K_d = 2-7 \mu\text{M}$

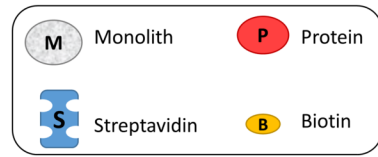
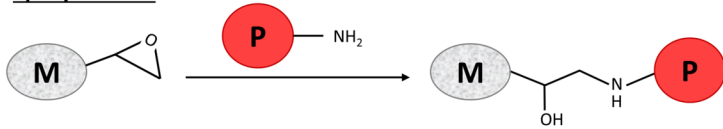


Furosemide
Site IIA
 $K_d = 5-50 \mu\text{M}$

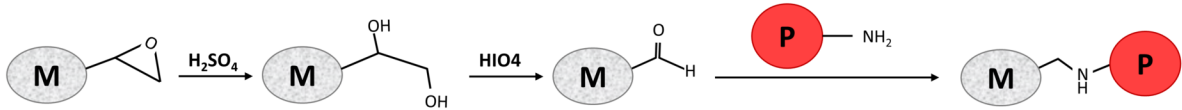


Ibuprofen
Site IIIA
 $K_d = 0.3-25 \mu\text{M}$

Epoxy method



Schiff base method



Streptavidin-biotin method

